Fuel 341 (2023) 127609

Contents lists available at ScienceDirect

Fuel

journal homepage: www.elsevier.com/locate/fuel

Full length article

Effects of water subdroplet location on the start of puffing/micro-explosion in composite multi-component fuel/water droplets

G. Castanet [a], D.V. Antonov [b], I.A. Zubrilin [c], P.A. Strizhak [b], S.S. Sazhin [d,*]

[a] Université de Lorraine, CNRS-UMR7563, CS 25233, France
[b] National Research Tomsk Polytechnic University, 30, Lenin Avenue, 634050, Tomsk, Russia
[c] Samara National Research University, 34, Moskovskoye Shosse, Samara 443086, Russia
[d] Advanced Engineering Centre, School of Architecture, Technology and Engineering, University of Brighton, Brighton, BN2 4GJ, UK

ARTICLE INFO

Keywords:
Composite droplets
Heating
Evaporation
Puffing
Micro-explosion
Multi-component fuel
Component diffusion equation

ABSTRACT

An earlier reported model for the prediction of the onset of puffing/micro-explosion in composite multi-component water/liquid fuel droplets is generalised to consider the shifting of the water subdroplet relative to the centre of the fuel droplet. The droplet heating and evaporation are described within the Abramzon and Sirignano model. The equations of heat conduction in the droplet and component diffusion inside the fuel shell are solved numerically assuming that the composition and temperature are uniform over the droplet surface but vary with time. The change in the droplet size due to thermal swelling is considered. The verification of the new model is performed by comparing its predictions with those of the previously developed numerical code, based on the analytical solutions to the heat transfer and component diffusion equations, and used at each timestep of the calculations, for the case of a perfectly centred water subdroplet. The coincidence of the results supports both approaches to the problem. The timing of puffing/micro-explosion is then evaluated for droplets of two kerosene surrogates for various positions of the water subdroplet. It is pointed out that shifts of the water subdroplet by less than 20% lead to a reduction in the time to puffing/micro-explosion of less than 5%. This justifies the applicability of the previously developed model that was based on the assumption that a water subdroplet is located exactly in the centre of the fuel droplet. The times to puffing/micro-explosion predicted by the model are validated using the in-house experimental data for kerosene surrogate droplets (SU1: n-decane, iso-octane and methylbenzene; SU12: iso-octane and methylbenzene).

1. Introduction

The importance of puffing (swelling and break-up of droplets into smaller droplets) and micro-explosion (break-up of droplets leading to formation of a cloud of aerosols) in composite water/fuel droplets has been widely described [1]. Puffing/micro-explosion is initiated when the temperature at the fuel–water interface becomes equal to the water nucleation temperature [2]. Models of various levels of complexity have been developed over the years to describe specific aspects of the phenomenon starting with the approaches based on DNS simulations [3–5] and ending with relatively simple models [1,6–9], which are expected to complement DNS models by highlighting the physical background of individual processes.

A simple model was developed by the authors of [7] for the case where a spherical water subdroplet is placed exactly in the centre of a spherical monocomponent fuel droplet. An analytical solution to the transient heat transfer equation was obtained for this problem and implemented into a numerical code. The effects of evaporation, using the model developed by Abramzon and Sirignano [10], and swelling were taken into account. The Robin boundary condition was adopted at the droplet surface to account for the convective heat fluxes at this boundary. Also, the retardation of the onset of puffing/micro-explosion by the superheating of water was taken into account based on the heating rate of the liquid at the interface between water and fuel.

In [6], this model was extended using a non-self-consistent approach to account for the effects of the droplet movement on Sherwood and Nusselt numbers but not on the liquid recirculation inside droplets. This extended model was shown to be effective in many applications including recent investigations of puffing/micro-explosion in two and three droplets in a row, one behind the other [11,12]. Heat and mass transfers within the gaseous phase were analysed separately assuming spatially uniform temperatures and vapour concentrations at the surface of the droplets in the row. Corrections to the Nusselt and Sherwood numbers, accounting for the spacing between the droplets, were formulated in [6].

* Corresponding author.
E-mail address: S.Sazhin@brighton.ac.uk (S.S. Sazhin).

https://doi.org/10.1016/j.fuel.2023.127609
Received 29 November 2022; Received in revised form 18 January 2023; Accepted 23 January 2023
0016-2361/© 2023 The Author(s). Published by Elsevier Ltd. This is an open access article under the CC BY license (http://creativecommons.org/licenses/by/4.0/).

Nomenclature

$B_{M(T)}$	Spalding mass (heat) transfer number [–]
c	Specific heat capacity [W/(kg K)]
D	Mass diffusion coefficient [m^2/s]
h	Convection heat transfer coefficient [W/(m^2 K)]
k	Thermal conductivity [W/(m K)]
L	Distance between the centres of water subdroplet and fuel droplet [m]
$\mathcal{L}$	Specific heat of evaporation [J/kg]
m	Mass [kg]
$\dot{m}_d$	Droplet evaporation rate [kg/s]
n	Normal to a surface [–]
Nu	Nusselt number [–]
Pr	Prandtl number [–]
$\dot{q}_d$	Heating rate [W]
r	Radial coordinate in the cylindrical reference system [m]
R	Distance from the droplet centre [m]
R_d	Droplet radius [m]
Re	Reynolds number [–]
S	$L/L_{\max}$ [–]
Sc	Schmidt number [–]
Sh	Sherwood number [–]
t	Time [s]
T	Temperature [K]
U	Velocity [m/s]
Y	Mass fraction [–]
z	Axial coordinate in the cylindrical reference system [m]

Greek symbols

$\alpha_{T(i)}$	Increment factor for the temperature T and the mass fraction Y_{li} [–]
β	Dilatation factor [–]
ϑ	Azimuthal coordinate in the cylindrical reference system [m]
ϵ_i	$\dot{m}_i/\dot{m}_d$ [–]
κ	Thermal diffusivity [m^2/s]
ρ	Density [kg/m^3]
τ_p	Time to puffing/micro-explosion [s]

Subscripts

av	Average
B	Boiling
d	Droplet
e	Evaporation
eff	Effective
f	Fuel
g	Ambient gas (air)
i	The ith component in the fuel
l	Liquid
max	Maximal
N	Nucleation
ref	Reference
s	Surface
v	Vapour
w	Water–fuel interface or water
0	Initial
1	At the end of the timestep, or specific component
∞	Ambient conditions

The model suggested in [7] was generalised by the authors of [9] to consider the contributions of multiple liquid components and relative diffusion between them. The same assumptions as in [7] were made in the new model except for that related to component diffusion. The analytical solutions to the equations for liquid fuel component diffusion were incorporated into the numerical code alongside the previously reported analytical solution to the temperature inside the composite droplet. Both solutions were used at each timestep of the calculation. Assuming an ideal mixture, Raoult's law was used at the surface of the droplet. It was shown that, for kerosene fuel, considering the presence of multiple components leads to an increase in the time to puffing/micro-explosion compared to the case when kerosene is approximated by one component (cycloundecane).

The model described in [9], however, has several weaknesses. It is based on the assumption that a spherical water subdroplet is located exactly in the centre of the fuel droplet. This results in an overestimate of the time required to attain the nucleation temperature at the water/fuel interface compared to the case when the location of the water subdroplet is shifted from the centre of the fuel droplet. To address this issue, the authors of [8] considered the effects of displacement of the water subdroplet. This generalisation (hereafter referred to as the Shift Model (SM)) was based on a purely numerical solution to the heat transfer equation in the fuel/water droplet using the finite element method with COMSOL multiphysics®. In this analysis of puffing/micro-explosion, the effects of mass loss due to fuel evaporation were ignored. The distance between the water/fuel interface and the outer surface of the fuel droplet was kept constant, which led to an overestimate of the time to puffing/micro-explosion. Also, the model described in [8] used the assumption that the fuel was a monocomponent fuel.

In the present study, the focus is on an extension of the SM model to consider the multi-component nature of the fuel (diffusion between fuel components). In contrast to [8], the implementation of the model in the numerical code considers the changes in droplet sizes due to evaporation and thermal swelling. This involves updates to the geometry of the composite droplet at each timestep of the calculations. A description of the new model and its implementation in the numerical code is presented in Section 2. The predictions of the model are compared with the predictions of the numerical code using the analytical solutions to heat transfer and component diffusion equations, developed by the authors of [9], in the case of a perfectly centred water subdroplet in Section 3. Estimates of the time to puffing/micro-explosion are made in the case of shifting of the water subdroplet for a wide range of ambient temperatures and droplet radii in Section 4. In Section 5, the predictions of the new model are compared with the results of experimental observations. For this comparison, two kerosene surrogates will be considered:

- a two-component fuel mixture named SU12 composed of iso-heptane and heptylbenzene with initial mass fractions $Y_{l10} = 0.691$ for iso-heptane and $Y_{l20} = 0.309$ for heptylbenzene.
- a three-component fuel mixture named SU1 composed of n-decane, iso-octane and methylbenzene with initial mass fractions $Y_{l10} = 0.4267$ for n-decane, $Y_{l20} = 0.3302$ for iso-octane and $Y_{l30} = 0.2431$ for methylbenzene.

The key findings of the paper are summarised in Section 6.

2. Description of the new model

The configuration considered for the geometry of the water/fuel droplet is the same as the one used in the Shift Model described in [8].

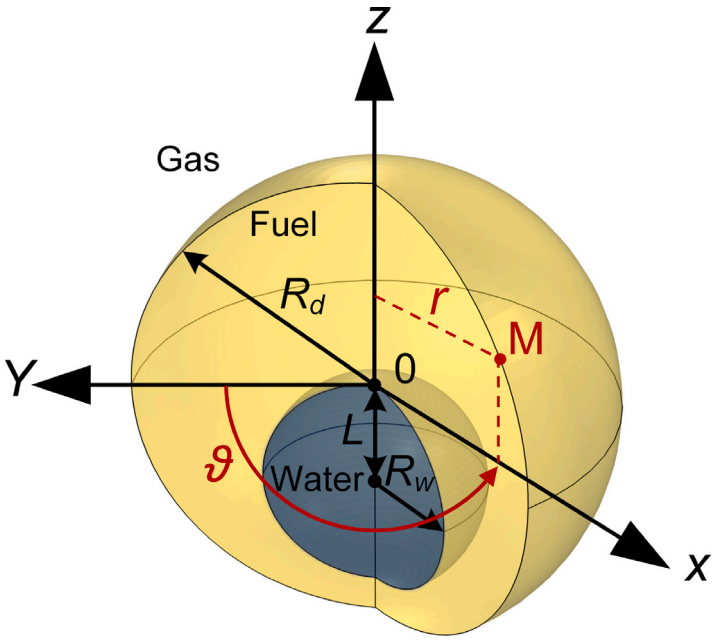

Fig. 1. Schematic presentation of the geometry and coordinates used in the Shift Model.

It is illustrated in Fig. 1. A spherical water subdroplet of radius R_w is shifted by a distance L from the centre of the spherical droplet of liquid fuel of radius R_d. In the case of a perfectly centred water subdroplet ($L = 0$), the modelling can be reduced to the analysis of the same set of equations as used in [9]. However, in the general case when the water subdroplet is shifted relative to the centre of the fuel droplet ($L \neq 0$), the problem needs to be reformulated. The cylindrical symmetry of the problem allows us to use the cylindrical coordinate system with the z-axis, being the line joining the centre of the fuel droplet to that of the water subdroplet, as presented in Fig. 1. The model considers the effects of heat transfer and component diffusion inside a composite water/fuel droplet. In what follows, the main equations and assumptions are described.

The heat conduction problem

Time and space evolution of the temperature inside a composite water/fuel droplet is described by the transient heat transfer equation:

$$\frac{\partial T}{\partial t} = \kappa \cdot \left(\frac{1}{r} \frac{\partial}{\partial r} \left(r \frac{\partial T}{\partial r} \right) + \frac{\partial^2 T}{\partial z^2} \right), \tag{1}$$

where

$$\kappa = \begin{cases} \kappa_w = k_w / \left(c_w \, \rho_w \right) & \text{in the water subdroplet} \\ \kappa_f = k_f / \left(c_f \, \rho_f \right) & \text{in the fuel shell} \end{cases} \tag{2}$$

$\kappa_{w(f)}$, $k_{w(f)}$, $c_{w(f)}$, and $\rho_{w(f)}$ are the water (fuel) thermal diffusivity, thermal conductivity, specific heat capacity, and density, respectively. Eq. (1) was solved numerically with the initial condition:

$$T|_{t=0} = \begin{cases} T_{w0}\,(r, z) & \text{in the water subdroplet} \\ T_{f0}\,(r, z) & \text{in the fuel region} \end{cases} \tag{3}$$

At the water/fuel interface, the continuity of the temperature and heat flux are presented as:

$$T_w = T_f, \quad k_w \frac{\partial T_w}{\partial n} = k_f \frac{\partial T_f}{\partial n}, \tag{4}$$

where n refers to the direction normal to the surface of the water subdroplet. The axi-symmetric configuration of the problem requires:

$$\left. \frac{\partial T}{\partial r} \right|_{r=0} = 0. \tag{5}$$

As in [8], it is assumed that the temperature at the surface of the fuel droplet is uniform although it may change with time:

$$\left. \frac{\partial T}{\partial z} \right|_{R=R_d} = 0, \tag{6}$$

where $R = \sqrt{r^2 + z^2}$ is the distance to the droplet centre. The change in the temperature with time is controlled by the average heating rate $\dot{q}_d$:

$$\int_{-R_d}^{R_d} \left. \frac{\partial T}{\partial R} \right|_{R=R_d^-} dz = \frac{\dot{q}_d}{2\pi R_d k_f}. \tag{7}$$

This heating rate is estimated as:

$$\dot{q}_d = 4\pi R_d^2 \, h \, \left(T_{\text{eff}} - T_s \right), \tag{8}$$

where h is the convection heat transfer coefficient and T_{eff} is an 'effective' ambient gas temperature which considers the effects of droplet evaporation:

$$T_{\text{eff}} = T_g + \frac{\rho_f \mathcal{L} \dot{R}_{d(e)}}{h}, \tag{9}$$

$\dot{R}_{d(e)} = |\dot{m}_d| / 4\pi\rho_f R_d^2$ considers the change in R_d due to evaporation, and $\mathcal{L}$ is the specific heat of fuel evaporation. In our study, the model suggested by Abramzon and Sirignano [10] is used to evaluate the evaporation rate $\dot{m}_d$ and the heat transfer coefficient h.

The component diffusion problem

In contrast to the original SM model proposed in [8], the model used in the present analysis takes into account the multi-component nature of fuel in the fuel shell surrounding the water subdroplet. The following equations for mass fractions $Y_{li} \equiv Y_{li}(t, r, z)$ inside the liquid fuel shell were used:

$$\frac{\partial Y_{li}}{\partial t} = D_l \cdot \left(\frac{1}{r} \frac{\partial}{\partial r} \left(r \frac{\partial Y_{li}}{\partial r} \right) + \frac{\partial^2 Y_{li}}{\partial z^2} \right), \tag{10}$$

where $i \geq 1$, D_l is the liquid fuel diffusivity which is assumed to be constant for all components. Eq. (10) was solved numerically using the following conditions at the inner and outer boundaries of the fuel shell. At the water–fuel interface, no fuel component can penetrate from the fuel shell into the water, which implies:

$$\frac{\partial Y_{li}}{\partial n} = 0. \tag{11}$$

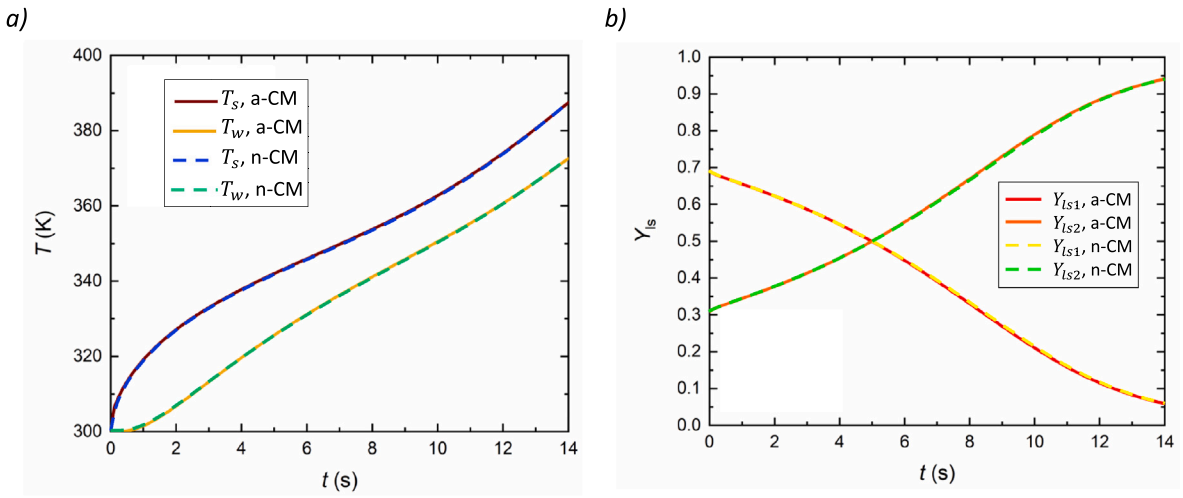

Fig. 2. Time evolution of a droplet made of SU12 and containing a water subdroplet perfectly positioned in the centre of the fuel droplet ($L = 0$). Parameters of the calculations are T_{d0} = 300 K, R_{d0} = 1 mm, T_g = 573 K. (a) Plots of droplet surface temperature (T_s) and the temperature at the fuel/water interface (T_w) versus time, (b) plots of liquid surface mass fractions of iso-heptane (Y_{ls1}) and heptylbenzene (Y_{ls2}) versus time.

The component diffusion equation was not solved inside the water subdroplet. The axi-symmetric configuration of the problem also requires:

$$\left.\frac{\partial Y_{li}}{\partial r}\right|_{r=0} = 0. \tag{12}$$

In line with the heat conduction problem, the mass fraction of all components is uniformly distributed over the outer boundary of the fuel shell:

$$\left.\frac{\partial Y_{li}}{\partial z}\right|_{R=R_d} = 0. \tag{13}$$

On the liquid side at $R = R_d^-$, the flow rate of component i can be written in terms of the mass fraction:

$$2\pi R_d \int_{-R_d}^{+R_d} -\rho_f D_l \left.\frac{\partial Y_{li}}{\partial R}\right|_{R=R_d^-} dz = \dot{m}_d \cdot \left(\epsilon_i - Y_{lis}\right), \tag{14}$$

where $Y_{lis} = Y_{lis}(t)$ are mass fractions of components i at the droplet surface. The flux of component i transferred to the droplet surface by diffusion from the bulk liquid fuel must compensate for the mass of the evaporated component. Assuming that all vapour components have the same diffusivity D_v, the contribution of component i to the global mass flux is proportional to its vapour mass fraction Y_{vis} at the droplet's surface:

$$\epsilon_i = Y_{vis} \Big/ \sum_i Y_{vis}\ . \tag{15}$$

The mass transfer problem was solved with the initial condition:

$$Y_{li}(r, z, t)\big|_{t=0} = Y_{li0}(r, z). \tag{16}$$

Implementation of the model

The modules "Transport of Diluted Species" and "Heat Transfer in Fluids" in COMSOL multiphysics® were used to numerically solve the heat transfer and component diffusion equations with appropriate initial and boundary conditions. There were some difficulties with satisfying the integral boundary conditions specified in Eqs. (7) and (14) due to the constraints of uniform temperature (T_s) and mass fraction (Y_{lis}) at the droplet surface. These difficulties were overcome by using the linearity of the heat and mass transfer problems. Both problems were decomposed into two sub-problems that were more straightforward to solve, with an imposed Dirichlet condition at the droplet surface. More details are provided in Appendix.

In contrast to [8], the time variations of $R_d(t)$ and $R_w(t)$ are taken into account in the numerical resolution. These are evaluated from the following equations:

$$\frac{4}{3}\pi \rho_{w1} {R_{w1}}^3 = \frac{4}{3}\pi \rho_{w0} {R_{w0}}^3, \tag{17}$$

$$\frac{4}{3}\pi \rho_{f1} \left({R_{d1}}^3 - {R_{w1}}^3\right) = \frac{4}{3}\pi \rho_{f0} \left({R_{d0}}^3 - {R_{w0}}^3\right) - \dot{m}_d\ dt, \tag{18}$$

where indices 0 and 1 refer to times t and $t + dt$. Average values of the temperature and the mass fraction in the fuel and water regions are used to evaluate the densities of water and fuel. At each timestep of the calculations, the following steps are performed. Eqs. (1) and (10) are solved in the old geometry corresponding to the state of the droplet evaluated at time t. The deformation of the composite droplet due to evaporation and thermal swelling is ignored during the timestep. Then, using Eqs. (17) and (18), the geometry of the droplet is updated considering the values obtained for $R_d(t + dt)$ and $R_w(t + dt)$. It is assumed that the centres of the water subdroplet and the fuel shell do not move (there is no relative displacement of the centres of the water subdroplet and fuel shell). A new mesh is generated considering the updated geometry at time $t+dt$. The fields of T and Y_{li} are interpolated at each node of this new mesh. This is done with the help of a dilatation factor $\beta = R_d(t+dt)/R_d(t)$ which is applied to maintain a perfect match between the solution and the surface of the droplet at $R = R_d(t + dt)$. Then, the calculations continue at the following timestep.

Finding the velocity field induced by the thermal swelling in the fuel shell is non trivial except in the case where the water subdroplet is positioned exactly at the centre of the fuel droplet. In our simulations, thermal swelling is taken into account by updating the values of R_d and R_w at each timestep, but the transport of heat and mass which results from the swelling is ignored. This simplification is supported by simulations performed taking into account the velocity field of the thermal swelling in the case of a centred water subdroplet. These show little effect due to thermal swelling on the time evolution of the temperature at the water/fuel interface in the conditions encountered in the experiments (see Fig. 4 in Section 3).

3. Verification of the model for a centred water subdroplet

The Shift Model (SM) reduces to the Centre Model (CM) used by the authors of [9] when the water subdroplet is perfectly centred ($L = 0$). Indeed, the spherical symmetry in that configuration results in a simplification of the boundary integral conditions (Eqs. (7) and (14)). Eq. (7) turns into the Robin condition as it was formulated in [9].

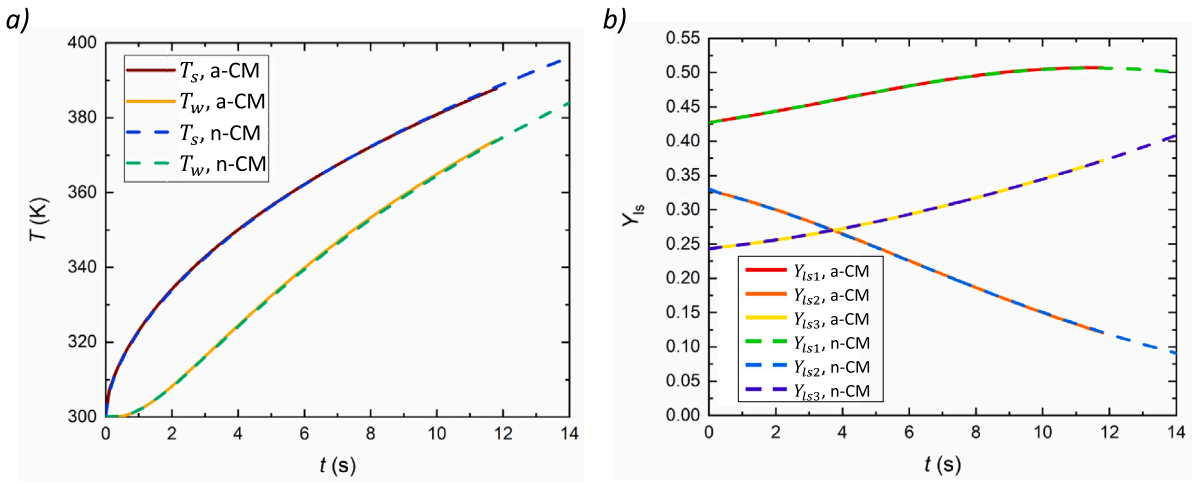

Fig. 3. Time evolution of a droplet made of SU1 and containing a water subdroplet perfectly positioned in the centre of the fuel droplet ($L = 0$). Parameters of the calculations are T_{d0} = 300 K, R_{d0} = 1 mm, T_g = 573 K. (a) Plots of droplet surface temperature (T_s) and the temperature at the fuel/water interface (T_w) versus time, (b) plots of liquid surface mass fractions of n-decane (Y_{ls1}), iso-octane (Y_{ls2}) and toluene (Y_{ls3}) versus time.

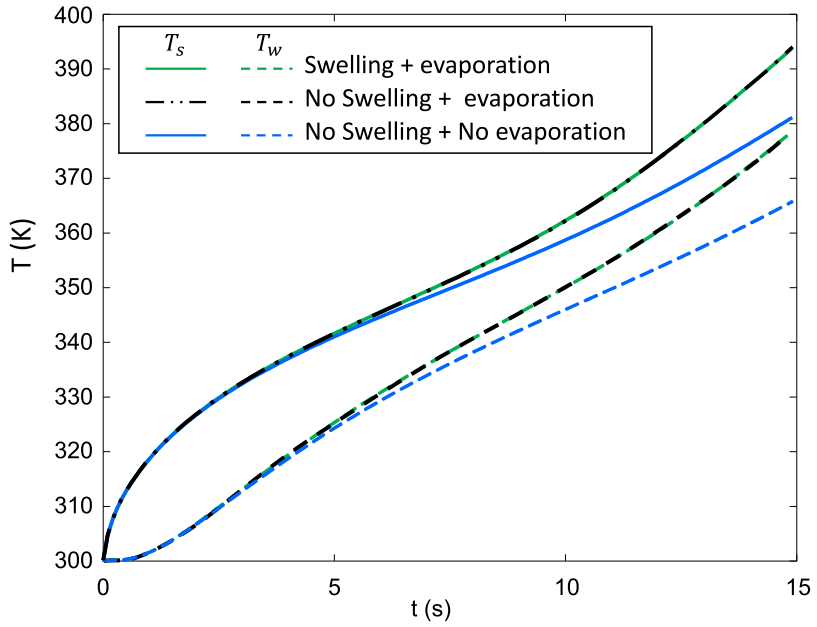

Fig. 4. Effect of thermal swelling and fuel evaporation on the evolution of droplet surface temperature and the temperature at the water/fuel interface for a droplet made of SU12. The parameters used in the simulation are the same as in Fig. 2. The n-CM approach was used.

The model based on the analytical solution to the heat transfer and component diffusion equations developed in [9] is hereafter referred to as 'a-CM'. The predictions of 'a-CM' were used to verify the purely numerical approach developed in the present study which is based on the numerical solution to the heat transfer and component diffusion equations, hereafter referred to as 'n-CM'. The following parameter values were set in this comparison:

- Initial droplet temperature T_{d0} = 300 K.
- Initial water volume fraction 10%.
- Ambiant pressure fixed at P = 101 325 Pa.

Figs. 2 and 3 show the time evolution of the temperatures at the droplet's surface (T_s) and the water/fuel interface (T_w) along with the mass fraction of the fuel components (Y_{lis}) at the droplet surface for both SU12 and SU1. Calculations were performed for ambient gas temperature of 573 K and initial radius of the composite droplet equal to 1 mm. As follows from Figs. 2 and 3, the results for both 'a-CM' and 'n-CM' coincide within the accuracy of plotting. This suggests that the code based on the numerical solutions to the heat transfer and component diffusion equations described in Section 2 and the code based on the analytical solutions to these equations are verified for this case. On the plots shown in Figs. 2 and 3, it can be clearly observed that the evolution of the surface temperature is not exactly the same for SU12 and SU1. Times to puffing/micro-explosion with these two kerosene surrogates are compared later for an extensive range of gas temperatures in Section 4.

In the case of a perfectly centred water subdroplet, the liquid flow induced by the thermal swelling could be accounted for rigorously in the numerical code. The result is presented for SU12 in Fig. 4 under the same conditions as in Fig. 2. The predictions are compared to the results of simulations performed ignoring mass change induced by fuel evaporation and/or thermal swelling. It can be seen in Fig. 4 that the results obtained with and without considering the effect of swelling are almost superimposed. Hence, thermal swelling has no noticeable effect

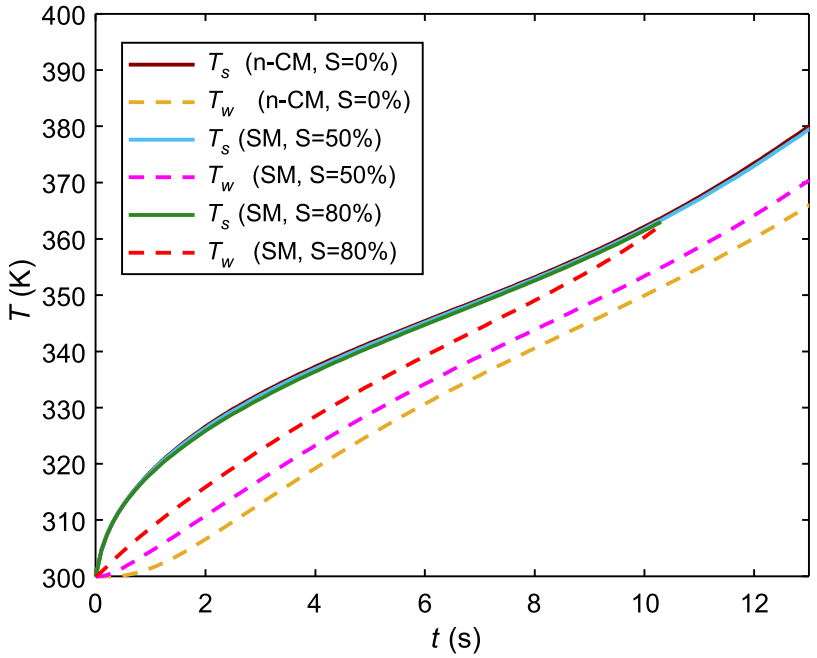

Fig. 5. Time evolution of the surface temperature (T_s) and the temperature at the water/fuel interface (T_w) for different shifts in the position of the water subdroplet for the case of two-component kerosene surrogate SU12. The same input parameters as in Figs. 2 and 4 were used.

on the temperature evolution at the fuel–water interface. Thus, its effect can be safely ignored when predicting the occurrence of puffing/micro-explosion. In contrast, ignoring the loss of mass due to evaporation results in a significant slow down in predicted droplet heating.

4. The effect of the water subdroplet location on the timing of puffing/micro-explosion

Simulations were carried out to clarify the effects of shifting in the position of the water subdroplet relative to the centre of the fuel droplet. Several parameters, such as the gas temperature (T_g) and the initial radius of the droplet (R_{d0}), were also examined. The shifting of the water subdroplet is described by parameter L, which is the distance between the centres of the water subdroplet and the fuel droplet, shown in Fig. 1. The maximal value of L is $L_{\max} = R_{d0} - (R_{w0}/2)$, where R_{d0} and R_{w0} are the initial values of fuel droplet and water subdroplet radii, respectively. For the present analysis, we introduced the normalised shift (S) defined as:

$$S = \frac{L}{L_{\max}}, \tag{19}$$

The size of the composite droplet changes with time and so does the value of L. It must be recalled that the normalised shift S is defined for the start of the droplet heating/evaporation when $R_d = R_{d0}$.

Nucleation of water can be delayed due to superheating. The water nucleation temperature T_N, at which puffing/micro-explosion is expected to be initiated, was approximated using the same model as in [7]:

$$T_N = T_B + 12 \times \tanh(\dot{T}/50); \qquad 0 \le \dot{T} \le 300 \ \text{K/s}, \tag{20}$$

$$T_N = 385 + 160 \times \tanh(\dot{T}/10^5) \qquad 10^2 \le \dot{T} \le 10^6 \ \text{K/s}, \tag{21}$$

$$T_N = T_B + 0.37 \times T_B \cdot \dot{T}^{10/Ja_{HN}} \qquad 10^5 \le \dot{T} \le 10^9 \ \text{K/s}, \tag{22}$$

where $Ja_{HN} = 626$ for water, T_B is the water boiling temperature, $\dot{T}$ is the rate of change of the temperature at the fuel/water interface.

4.1. Puffing/micro-explosion in droplets made of water and SU12

Fig. 5 presents the time evolution of the temperatures for the two-component kerosene surrogate SU12 droplet. The conditions are the same as in the previous examples ($R_{d0} = 1$ mm and $T_g = 573$ K), but different values of the normalised shift S are now considered: $S = 0$, $S = 0.5$ and $S = 0.8$. The temperature T_w is evaluated at the point of the water/fuel interface with the shortest distance to the external surface of the fuel shell. Shifting the position of the water droplet has almost no effect on the time evolution of the surface temperature. However, it accelerates the rise in temperature T_w at the water–fuel interface and thus leads to an earlier start to puffing/micro-explosion. This is illustrated in Fig. 6 where the spatial distributions of the temperature and the mass fraction of iso-heptane inside the droplet are shown at $t = 10$ s. Heat penetration into the core of the droplet is more efficient for the case when $S = 0.8$. The outer circle plotted in black shows the initial position of the droplet surface. As the fuel vapour is progressively released, the external surface of the droplet shrinks and moves closer to the water/fuel interface. For $S = 0.8$, the water/fuel interface reaches the external surface shortly after $t = 10$ s. The simulation is then stopped as this scenario is not expected to lead to puffing/micro-explosion.

The effect of the gas temperature T_g on predicted time to puffing/micro-explosion is illustrated in Fig. 7. The initial droplet radius R_{d0} is assumed equal to 1 mm. The nucleation temperature T_N evaluated by Expression (20) exceeds the saturation boiling temperature by only a few K. An increase in the gas temperature for $S = 0$ (perfectly centred water subdroplet) leads to a sharp decrease in the time to puffing/micro-explosion as illustrated in Fig. 7a. The effect of shifting the water subdroplet position relative to the centre of the fuel droplet is shown in Fig. 7b. As expected, the larger the normalised shift S, the earlier puffing/micro-explosion is predicted. It is observed that increasing S leads to a more pronounced reduction in the time to puffing/micro-explosion (τ_p) when the gas temperature increases. As already pointed out by Castanet et al. [8], the shift S has a moderate effect on τ_p (typically less than 10%) when S is limited to 0.5. Due to the shrinkage of the droplet, τ_p could not be evaluated when S

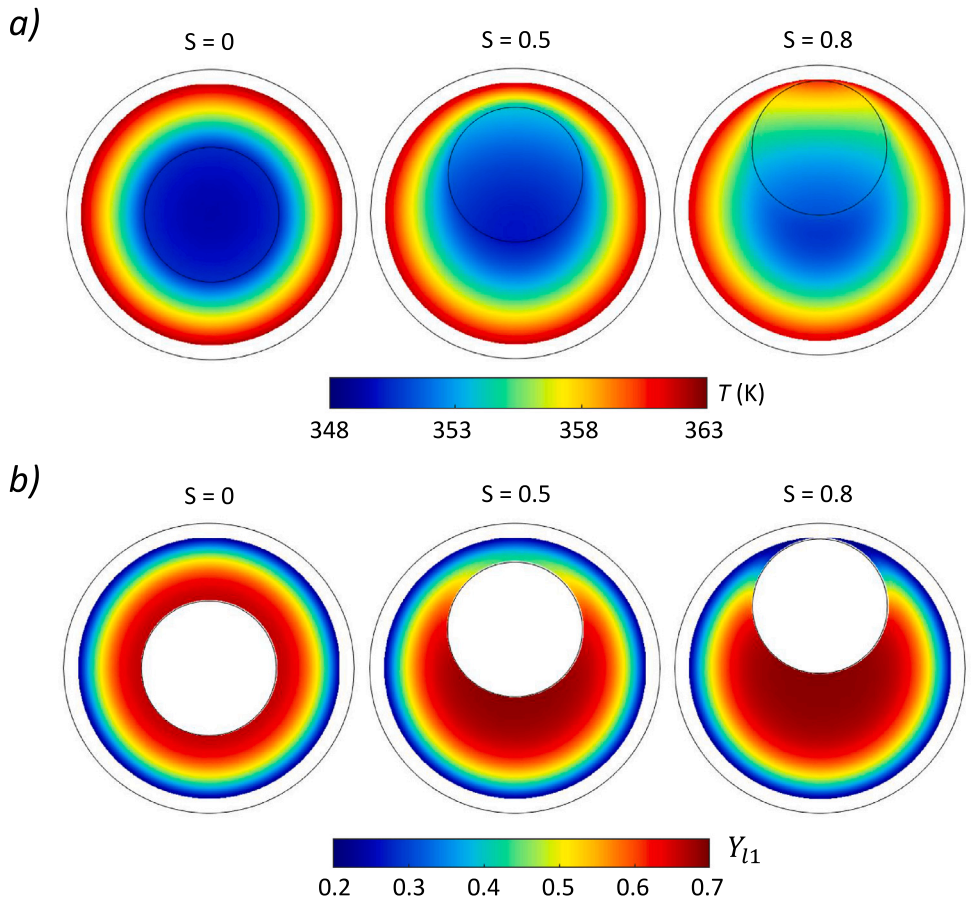

Fig. 6. Maps of temperature distribution (a) and iso-heptane mass fraction (b) at t = 10 s for three shifts in the position of the water subdroplet for the case of two-component kerosene surrogate SU12. The same input parameters as in Fig. 5 were used.

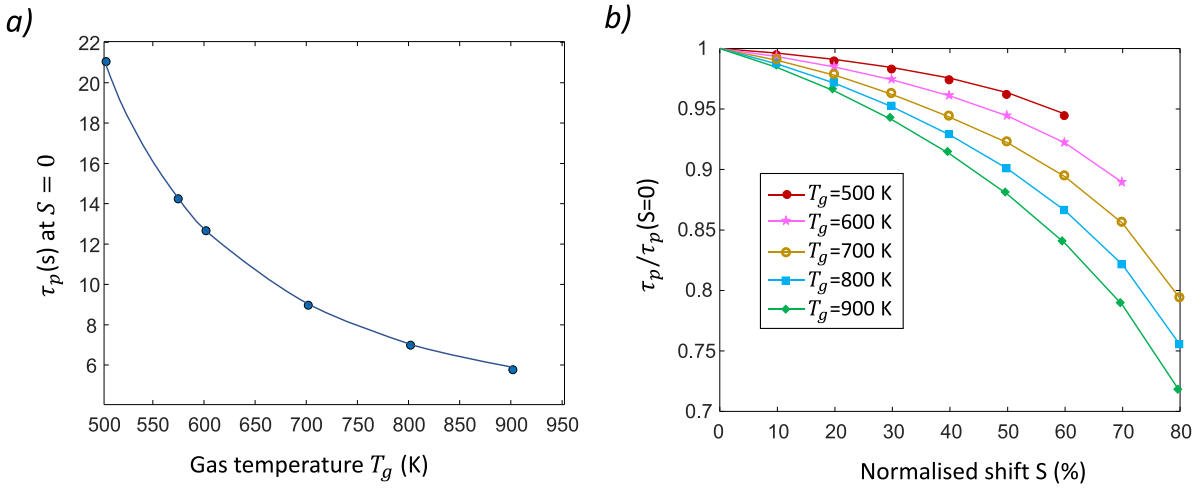

Fig. 7. Times to puffing/micro-explosion at gas temperatures T_g (500 K, 573 K, 600 K, 700 K, 800 K, 900 K) in the case of a perfectly centred water subdroplet (S = 0) (a). Relative times to puffing/micro-explosion versus S for the five gas temperatures (b). Calculations were performed for droplets composed of water and SU12 with initial radii R_{d0} = 1 mm.

exceeds 0.8 for any of the gas temperatures tested. For high values of S, the external surface of the composite droplet reaches the water/fuel interface before nucleation takes place.

The effect of shifting the position of the water droplet on the values of T_s and T_w is shown in Fig. 8b for several initial droplet radii R_{d0} ranging from 10 μm to 1 mm. The gas temperature T_g was assumed equal to 700 K. As expected, the smaller the initial droplet radius, the faster is the predicted droplet heating and thus puffing/micro-explosion is expected to occur earlier (Fig. 8a). Decreasing the initial droplet radius R_{d0} by a factor of 100, reduces the time to puffing/micro-explosion by more than 1000. As follows from Fig. 8b, the effect of S is almost the same for all droplet sizes when R_{d0} is greater than 0.1 mm. However, some noticeable differences can be seen for the smallest droplets (R_{d0} = 10 μm). For very small droplets, the nucleation

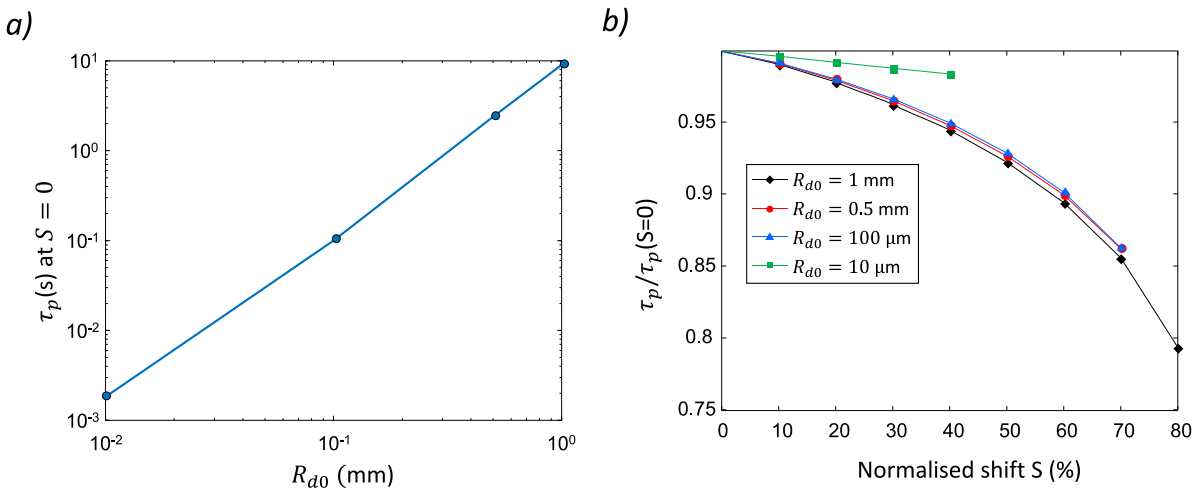

Fig. 8. Times to puffing/micro-explosion at initial radii R_{d0} (0.01 mm, 0.1 mm, 0.5 mm, 1 mm) for T_g = 700 K and $S = 0$ (a). Variation of the time to puffing/micro-explosion with S (b). Calculations were performed for droplets composed of water and SU12.

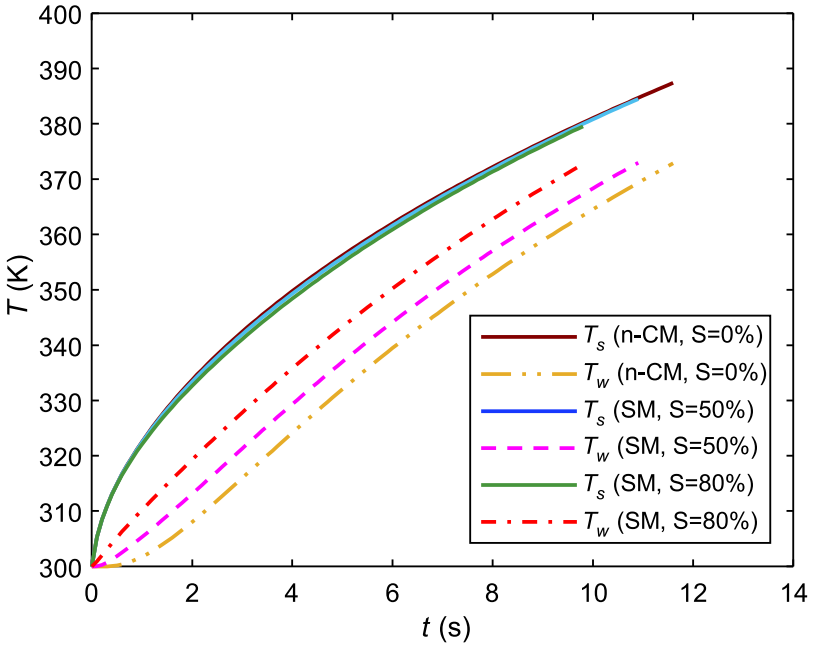

Fig. 9. Time evolution of the surface temperature (T_s) and the temperature at the water/fuel interface (T_w) for three shifts of the water subdroplet from the centre of the fuel droplet for the case of three-component surrogate SU1. Input parameters are the same as in Figs. 2 and 4.

temperature T_N can be as large as 500–550 K, according to Expression (22), which results in a significant delay in the start of puffing/micro-explosion. Fig. 8b also shows that S has a limited influence on the timing of puffing/micro-explosion for droplets in the micron size range.

4.2. Puffing/micro-explosion in droplets of water and SU1

For three-component mixture SU1, simulations were also carried out for various shifts in the position of the water subdroplet, initial droplet radii and gas temperatures. In Fig. 9, the time evolution of the temperature at the droplet surface (T_s) and at the fuel/water interface (T_w) is presented for three values of S at T_g = 573 K and R_{d0} = 1 mm. Shifting the position of the water subdroplet has a clear effect on the temperature at the fuel/water interface T_w, but very little effect on the temperature T_s.

When the gas temperature T_g and the initial radius R_{d0} are changed, similar trends to those already observed with the two-component fuel SU12 can be clearly seen in Figs. 10 and 11. As follows from the results shown in Fig. 10, the higher the ambient gas temperature, the more important is the effect of S on the timing of puffing/micro-explosion. Droplets composed of SU1 heat up at a slightly faster rate than those composed of SU12, which results in slightly earlier puffing/micro-explosion. For this reason, τ_p could be evaluated for values of S as large as 0.9.

In Fig. 11, the effect of S on time to puffing/micro-explosion is illustrated for initial droplet radii ranging from 10 µm to 1 mm at a fixed gas temperature T_g = 700 K. The results shown in this figure are very similar to those presented for SU12 in Fig. 8. As follows from Fig. 11, for R_{d0} larger than 0.1 mm the effect of S on time to puffing/micro-explosion is the same, regardless of the droplet radius, as long as the superheating of water remains moderate. For very small droplets ($R_{d0} \leq 10$ µm), changing the position of the water droplet has a very small effect on the time to puffing/micro-explosion. In the latter case, however, the external surface of the droplet reaches the fuel–water interface before puffing/micro-explosion occurs for S as small as 0.5.

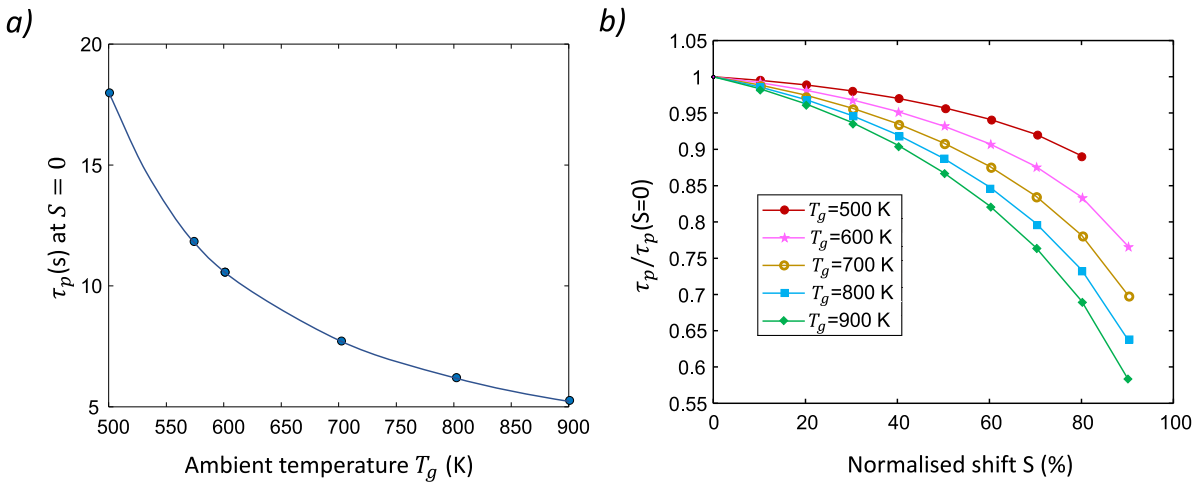

Fig. 10. Times to puffing/micro-explosion at six gas temperatures T_g (500 K, 573 K, 600 K, 700 K, 800 K, 900 K) for a perfectly centred water subdroplet, $S = 0$ (a). Relative times to puffing/micro-explosion versus S at five gas temperatures (b). Calculations were performed for droplets composed of water and SU1 with initial radii R_{d0} = 1 mm.

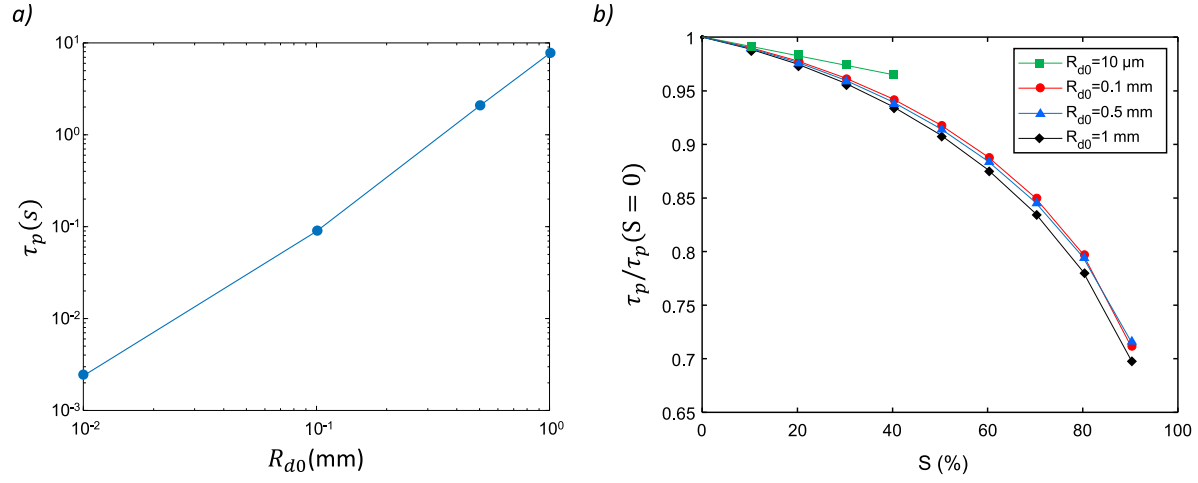

Fig. 11. Times to puffing/micro-explosion at initial radii R_{d0} (0.01 mm, 0.1 mm, 0.5 mm, 1 mm) for T_g = 700 K (a). Normalised times to puffing/micro-explosion versus S (b). Calculations were performed for droplets of water and SU1.

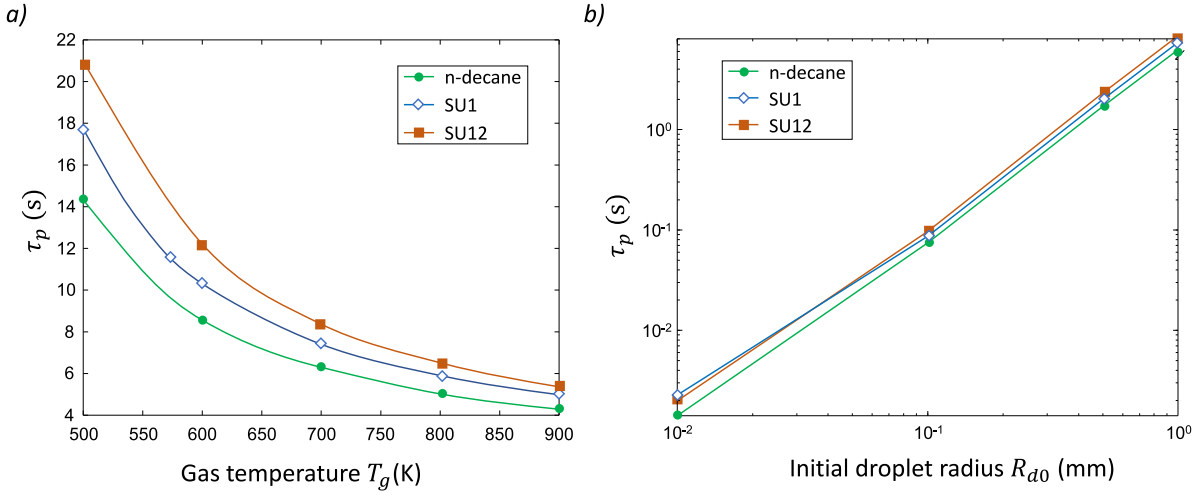

Fig. 12. Time to puffing/micro-explosion versus the gas temperature for a water subdroplet located at $S = 0.3$ (a), effect of the initial droplet size on time to puffing/micro-explosion (b). Calculations were performed for three kerosene surrogates (n-decane, SU1 and SU12).

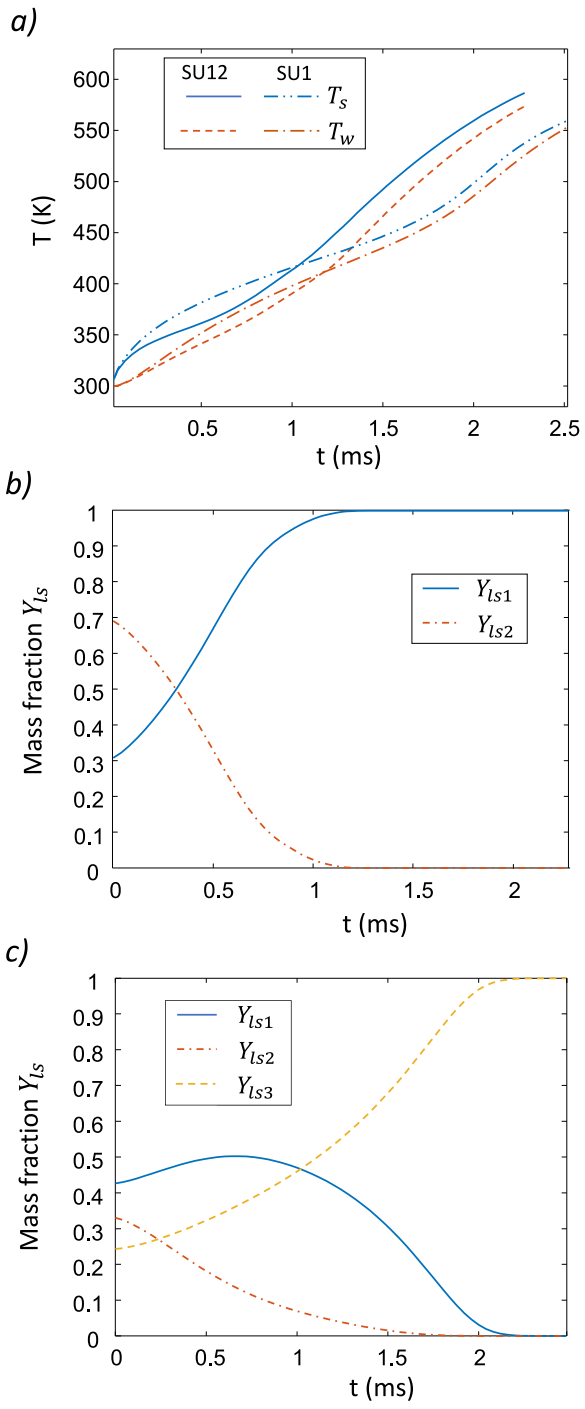

Fig. 13. Time evolution of the surface temperature (T_s) and the temperature at the water/fuel interface (T_w) for kerosene surrogates SU1 and SU12 (a), time evolution of the surface mass fractions of heptylbenzene (Y_{ls1}) and iso-heptane (Y_{ls2}) for SU12 (b), time evolution of the surface mass fractions of n-decane (Y_{ls1}), iso-octane (Y_{ls2}) and toluene (Y_{ls3}) for SU1 (c). Calculations were performed for S = 0.3, T_g = 700 K and R_{d0} = 10 μm.

4.3. Comparison of the effects of different kerosene surrogates

A comparison between the predicted times to puffing/micro-explosion at various gas temperatures and initial droplet radii for kerosene surrogates SU1 and SU12 (considered earlier) and n-decane (the simplest kerosene surrogate), is shown in Fig. 12. The curves are

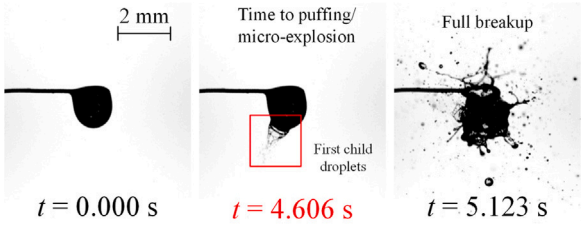

Fig. 14. Typical dynamics of puffing/micro-explosion in the experiments performed at National Research Tomsk Polytechnic University. A surrogate SU1/water droplet with an initial radius R_{d0} = 0.95 mm and volume fraction of water of 10 ± 2% was placed in an air flow of constant velocity U_g = 3.1 ± 0.1 m/s at atmospheric pressure and gas temperature T_g = 530 ± 3 K. t = 0 s refers to the time instant when the droplet was placed in the air flow.

presented for S equal to 0.3. In Fig. 12a, the time to puffing/micro-explosion (τ_p) is presented as a function of the gas temperature (T_g) for an initial radius R_{d0} = 1 mm. As expected, τ_p decreases with T_g for all the surrogates considered, but there are differences in the values of τ_p obtained. Puffing/micro-explosion is predicted to occur with the shortest delay for pure n-decane and with the longest delay for SU12. These differences decrease when gas temperature increases but they are still clearly seen at T_g = 900 K ($\tau_p \approx$ 4.1 s for n-decane against 5.8 s for SU12 and 5 s for SU1). The differences in τ_p shown in Fig. 12a seem to be closely correlated to the volatility of the surrogate compounds. In the two-component mixture SU12, iso-heptane has a lower boiling point compared to the compounds of SU1 (n-decane, iso-octane and toluene). Its faster evaporation, given the latent heat it consumes, is expected to slow down the heating rate of the droplet more than this is expected to happen for the other surrogates. Therefore, a longer time is required for SU12 to reach the nucleation temperature of water compared to other surrogates. In the case of SU1, the evaporation of iso-octane prevails over the two other compounds of the mixture (n-decane and toluene) at the start of heating, which leads to a slower heating rate compared to the case of pure n-decane.

The differences in times to puffing/micro-explosion predicted for three surrogates can be clearly seen in Fig. 12a for all initial droplet sizes. Note that for very small droplets (R_{d0} = 10 μm), τ_p becomes smaller for SU12 than for SU1. These cases are shown in more detail for both mixtures in Fig. 13, where the time evolution of temperature and mass fractions of the surrogate compounds are presented. For droplets in the μm size range, the heating rate is very high and the nucleation temperature of water T_N rises dramatically. The temporal evolution of the temperature at the droplet surface and the temperature at the fuel/water interface are shown in Fig. 13a for an initial droplet radius R_{d0} equal to 10 μm and T_g = 700 K for both SU1 and SU12. In this case, $\dot{T}_w$ is of the order of 10^5 K/s, and the nucleation temperature of water is close to 530 K. Until about t = 1.2 ms, T_s and T_w are highest for the two-component surrogate SU12, then the situation changes. Fig. 13b shows that the mass fraction of the most volatile compounds of SU12 (iso-heptane) tends towards 0 at the droplet's surface when the surface temperature exceeds about 420 K for SU12 which takes place at about t = 1.2 ms. In Fig. 13c, the most volatile compound of SU1, iso-octane, disappears from the droplet surface a little later, at about 1.7 ms, when T_s reaches about 440 K. Because of the lower volatility of the remaining compounds, an accelerated heating is observed when the low volatility compounds become extinct at the droplet surface for both SU1 and SU12. The depletion of the most volatile compound at the droplet surface occurs earlier in the case of SU12. This is why τ_p becomes significantly smaller for SU12 when R_{d0} = 10 μm.

5. The predictions of the model versus experimental data

In this section, the predictions of the new model are compared with experimental data obtained at National Research Tomsk Polytechnic

Table 1
Times to puffing/micro-explosion (τ_p) observed experimentally (Exp) and predicted by the new model for monocomponent (n-decane) and multi-component (SU1) surrogates, for ten cases, with the values of R_{d0}, T_g, U_g and S shown in the table. In all cases, the initial droplet temperature was 300 K, volume fraction of water was 0.1, and ambient gas pressure was atmospheric. The predicted values of τ_p closest to experimental data are highlighted in bold.

Case	R_{d0} (mm)	T_g (K)	U_g (m/s)	S	τ_p (s) (Exp)	τ_p (s) (n-decane)	τ_p (s) (SU1)
1	0.92	433	2.8	0.42	8.928	∞	**8.445**
2	0.95	433	2.8	0.54	9.016	∞	**8.584**
3	0.95	530	3.1	0.48	4.606	**4.395**	4.154
4	0.90	530	3.1	0.72	4.050	**3.329**	3.220
5	0.89	595	3.1	0.75	3.240	**2.367**	2.323
6	0.95	595	3.1	0.44	3.840	**3.475**	3.336
7	0.95	541	3.8	0.50	4.185	**3.956**	3.717
8	0.83	541	3.8	0.22	3.564	**3.508**	3.309
9	0.87	532	5.3	0.10	3.682	3.824	**3.514**
10	0.99	532	5.3	0.35	4.508	**4.449**	4.054

University for kerosene surrogate SU1. The experiments took place in a heated air flow where the droplets were supported by a nickel–chromium alloy wire of 0.2 mm diameter as in the experimental setup described in [13]. The initial droplet temperature was 300 ± 3 K; the initial droplet radii were in the range 0.83 mm to 0.99 mm; the systematic errors of droplet radii measurements were ±0.05 mm. The water volume fraction was 10 ± 2% in all experiments. The ambient pressure was atmospheric, taken equal to 101 325 Pa; the gas temperatures were in the range 433 K to 595 K; the systematic errors of gas temperature measurements were ±3 K; the gas velocities U_g were in the range 2.8 m/s to 5.3 m/s; the systematic errors of their measurements were ±0.1 m/s. The normalised shifts S were in the range 0 to 0.75; the systematic errors of their measurements were equal to ±5%. The details of the measurement procedure of the values for R_{d0}, T_g, U_g and S can be found in [8]. The times to puffing/micro-explosion in the experiments were estimated as times from the start of droplet heating to times when child droplets were first observed in videoframes. The systematic errors of times to puffing/micro-explosion measurement were ±0.002 s. Typical images are shown in Fig. 14.

The location of the water subdroplet inside the fuel droplet was identified before the start of heating. Special care was taken to evaluate the shifting of the water subdroplet in the experiments, which was achieved using a combination of planar laser-induced fluorescence (PLIF) and shadowgraphy techniques [8]. The PLIF techniques allowed us to illuminate the water subdroplet. Shadowgraphy allowed us to illuminate both water subdroplet and fuel shell. The centres of the water subdroplet and fuel shell were determined using an in-house image analysis programme based on Matlab software and its image processing toolbox (see [8] for the details). During experiments, the location of the water subdroplet was not controlled.

When applying the new model to the analysis of experimental data, effects of forced convection had to be taken into account due to gas velocities in the range 2.8 m/s to 5.3 m/s. Convection effects were considered using the same assumptions as made in [6]. Nusselt (Nu) and Sherwood (Sh) numbers were evaluated using the following formulae:

$$Nu = \left[2 + \frac{\left(Nu_0 - 2\right)}{\left(1 + B_T\right)^{0.7} \cdot \frac{\ln(1+B_T)}{B_T}}\right] \cdot \frac{\ln\left(1 + B_T\right)}{B_T}, \tag{23}$$

$$Sh = \left[2 + \frac{\left(Sh_0 - 2\right)}{\left(1 + B_M\right)^{0.7} \cdot \frac{\ln(1+B_M)}{B_M}}\right] \cdot \frac{\ln\left(1 + B_M\right)}{B_M}, \tag{24}$$

where $Nu_0 = 1 + (1 + Re \cdot \mathrm{Pr})^{1/3} \cdot \max\left(1, Re^{0.077}\right)$ and $Sh_0 = 1 + (1 + Re \cdot Sc)^{1/3} \cdot \max\left(1, Re^{0.077}\right)$. The observed times to puffing/micro-explosion are presented in Table 1 for ten cases. Each of ten experiments, the results of which are presented in this table, were performed once. It was not possible to reproduce the same degree of shift of the water subdroplets in different experiments. Each experiment was accurately analysed to provide all input parameters for the model. The calculations were performed for two cases. Firstly, actual composition of SU1 was taken into account. Secondly, SU1 was approximated by n-decane.

As follows from this table, the values of τ_p predicted taking into account actual SU1 composition are always lower than those predicted for n-decane. At moderate gas temperatures, it is particularly important to take into account the multi-component nature of fuel. For T_g = 433 K, droplets composed of n-decane reach an equilibrium temperature of 370 K after about 13 s, and therefore puffing/micro-explosion is not expected to take place for these droplets while puffing is observed experimentally. On the other hand, considering SU1 as a fuel allows us to predict the occurrence of puffing/micro-explosion with accurate values of τ_p. In several cases, predictions for n-decane were closer to the measurement results than those for SU1, but the difference between them was within experimental uncertainties. Discrepancies between simulations and measurements may be due to complex effects that are not considered in the current model. In particular, a more accurate description of forced convection, especially a non-uniform temperature along the droplet surface, would have been beneficial for modelling [14,15].

6. Conclusions

An earlier reported model for the puffing and micro-explosion of composite multi-component water/liquid fuel droplets was generalised to consider the shifting of the water subdroplet relative to the centre of the fuel droplet. The droplet heating and evaporation were described using the Abramzon and Sirignano model. Droplet swelling and the component diffusion in the fuel shell were considered. The equations for heat conduction and component diffusion inside the droplet were solved numerically assuming that the composition and the temperature are uniform over the droplet surface but vary with time. This model can be considered at a generalisation of the similar model for monocomponent water/fuel composite droplets previously developed in [8].

The model was applied to the investigation of the onset of puffing/micro-explosion in composite droplets of two kerosene surrogates developed at Samara National Research University: three component mixture SU1 (n-decane, iso-octane and methylbenzene) and two-component mixture SU12 (iso-heptane and heptylbenzene).

The newly developed model was verified based on the comparison of its predictions with those of the previously developed numerical code based on the analytical solutions to the heat transfer and component diffusion equations, used at each timestep of the calculations, for the case of a perfectly centred water droplet. The start of the puffing/micro-explosion process was associated with the time instant when the temperature at the point of the water/fuel interface closest to the surface of the droplet reached the nucleation temperature of water. The coincidence of the results supported both approaches to the problem.

The timing of puffing/micro-explosion was then evaluated for various positions of the water subdroplet. Shifting the water subdroplet location resulted in a reduction in the time to puffing/micro-explosion, which was particularly noticeable for high gas temperatures and large normalised shifts. It was demonstrated that for normalised shifts of not more than 20% the reduction in the time to puffing due to the shifting of the water subdroplet did not exceed 5% for all ambient gas temperatures under consideration (up to 900 K). This supports the applicability of the earlier developed model that was based on the assumption that the water subdroplet is located exactly in the centre of the fuel droplet.

The model was validated based on in-house experimental results obtained at Tomsk Polytechnic University. The validation was performed for surrogate SU1 and n-decane. The initial droplet temperature used in the experiments was 300 K, volume fraction of water was 0.1, and ambient gas pressure was atmospheric. Good agreement between the predicted and observed times to puffing was demonstrated in most cases. In several cases, predictions for n-decane were closer to the measurement results than those for SU1, but the difference between n-decane and SU1 results was within experimental uncertainties. For moderate gas temperatures (433 K), calculations with n-decane were not able to predict the occurrence of puffing/micro-explosion, while this limitation is not observed for the multi-component fuel

CRediT authorship contribution statement

G. Castanet: Conceptualization, Methodology, Resources, Investigation, Software, Writing – review & editing. **D.V. Antonov:** Conceptualization, Methodology, Resources, Investigation, Software. **I.A. Zubrilin:** Resources, Investigation. **P.A. Strizhak:** Supervision, Resources, Investigation. **S.S. Sazhin:** Supervision, Conceptualization, Methodology, Writing – review & editing.

Data availability

Data will be made available on request.

Acknowledgements

The authors are grateful to the Tomsk Polytechnic University (TPU) development program, Priority 2030 (Priority-2030-NIP/EB-038-1308-2022) which supported D. Antonov, P.A. Strizhak, and S.S. Sazhin, and to the Russian Science Foundation (Grant 21-19-00876, https://rscf.ru/en/project/21-19-00876/) which supported I. Zubrilin.

Appendix

In the frame of the quasi-steady theory [10], conditions at the droplet surface (T_s and Y_{lsi}) are required to predict droplet heating and evaporation. The evaporation rate is given by the following formula [16]:

$$\dot{m}_d = -4\pi R_d\, \rho_{tot}\, D_v \ln\left(1 + B_M\right), \tag{25}$$

where the Spalding mass transfer number B_M is defined as

$$B_M = \frac{Y_{vs} - Y_{v\infty}}{1 - Y_{vs}}, \tag{26}$$

$Y_{vs} = \sum_i Y_{vis}$. Using Eq. (14), the mass balance applied to the ith component in the fuel yields:

$$m_i\,(t + dt) = m_i\,(t) + \dot{m}_d \cdot \left(\epsilon_i - Y_{lis}\right) \cdot dt. \tag{27}$$

The heat balance provides an expression for the evolution of the averaged temperature T_d of the composite droplet,

$$T_d(t + dt) = T_d(t) + \frac{\dot{q}_d}{m_f \cdot c_f + m_w \cdot c_w} \cdot dt, \tag{28}$$

where the rate at which heat enters the droplet $\dot{q}_d$ can be evaluated by Eq. (8). m_f and m_w are the mass of fuel and water in the droplet, respectively.

Eqs. (27) and (28) allow us to determine the temperature and the average mass fraction of the components at the next timestep of the calculation. To obtain the spatial distribution of these quantities, it is necessary to solve the equations of heat conduction (Eq. (1)) and component diffusion (Eq. (10)) with the associated boundary conditions. Assuming that the distribution of the temperature $T(r, z, t)$ and the mass fraction of components $Y_{li}(r, z, t)$ are known at a certain time t_0, they can be presented at the next timestep $(t_0 + dt)$ as a linear combination of two functions:

$$T\,(r, z, t) = T^a\,(r, z, t) + \alpha_T \cdot T^b\,(r, z, t)\,. \tag{29}$$

$$Y_{li}\,(r, z, t) = Y_{li}^a\,(r, z, t) + \alpha_i \cdot Y_{li}^b\,(r, z, t)\,. \tag{30}$$

The advantage of this decomposition is that the functions (T^a, T^b) for the heat transfer and (Y_{li}^a, Y_{li}^b) for the component diffusion are more straightforward to solve with an appropriate Dirichlet condition at the droplet surface.

Solution of the heat transfer problem

Both functions T^a and T^b are obtained by solving the heat transfer equation. They satisfy the axi-symmetry conditions (5). T^a is the solution to a modified problem where the surface temperature does not vary during the timestep between t_0 and $t_0 + dt$:

$$T^a\left(R = R_d, t\right) = T\left(R = R_d, t_0\right), \quad \text{for} \quad t_0 \le t \le t_0 + dt. \tag{31}$$

At time t_0, the initial value of the function T^a is obtained as:

$$T^a\left(r, z, t_0\right) = T\left(r, z, t_0\right), \tag{32}$$

where $T\left(r, z, t_0\right)$ is the temperature distribution in the droplet at the last timestep of the solution.

The function T^b represents the effect of a temperature increment of 1 K at the droplet surface. This function follows from the boundary (surface) and initial conditions:

$$T^b\left(R = R_d, t\right) = 1, \quad \text{for} \quad t_0 \le t \le t_0 + dt \tag{33}$$

$$T^b\left(r, z, t_0\right) = 0 \tag{34}$$

Finally, the temperature (solution to the heat conduction problem) is evaluated from Expression (29) using the above-mentioned values of T^a and T^b. The boundary condition (6), corresponding to a uniform surface temperature, is automatically satisfied. The parameter α_T in Eq. (29) can be determined whilst satisfying the integral boundary condition (7). Also, it can be inferred from the average temperature T_d given in Eq. (28) as a reference target:

$$\alpha_T = \frac{T_d\left(t_0 + dt\right) - T_d^a(t_0 + dt)}{T_d^b(t_0 + dt)}, \tag{35}$$

where T_d^a and T_d^b are the average values of T^a and T^b over the entire volume of the droplet.

Solution of the component diffusion problem

Functions Y_{li}^a and Y_{li}^b are obtained by solving the component diffusion equation. They satisfy the axi-symmetry conditions (12) and the condition of zero component mass flux at the fuel/vapour interface (Eq. (11)). Y_{li}^a is the solution to a modified problem where the mass fraction at the droplet surface Y_{lis} does not vary during the timestep between t_0 and $t_0 + dt$:

$$Y_{li}^a\left(R = R_d, t\right) = Y_{li}\left(R = R_d, t_0\right), \quad \text{for} \quad t_0 \le t \le t_0 + dt. \tag{36}$$

At time t_0, the initial value of the function Y_{li}^a is obtained as:

$$Y_{li}^a\left(r,z,t_0\right) = Y_{li}\left(r,z,t_0\right), \tag{37}$$

where $Y_{li}\left(r,z,t_0\right)$ are the distributions of the mass fractions of the ith compounds at the last timestep of the solution.

The function Y_{li}^b represents the solution to the component diffusion problem in a droplet that does not initially contain the components i. This function follows from the boundary (surface) and initial conditions:

$$Y_{li}^b\left(R = R_d, t\right) = 1, \quad \text{for} \quad t_0 \le t \le t_0 + dt \tag{38}$$

$$Y_{li}^b\left(r,z,t_0\right) = 0. \tag{39}$$

Finally, the component mass fraction Y_{li} (solution to the component diffusion problem) is evaluated from the values of Y_{li}^a and Y_{li}^b using Eq. (30). The parameter α_i in Eq. (30) can be determined whilst satisfying the boundary condition (14). Also, Eq. (27) can be used to evaluate the mass $m_i(t_0+dt)$ of the ith component. Then, α_i is estimated as:

$$\alpha_i = \frac{m_i\left(t_0+dt\right) - m_i^a(t_0+dt)}{m_i^b(t_0+dt)}, \tag{40}$$

where m_i^a and m_i^b are the mass fractions of the components i corresponding to the fields Y_{li}^a and Y_{li}^b.

Implementation in the numerical code

The mesh in the numerical solution was composed of about 250,000 structured quadrangle elements in the fuel region of the computational domain, and 10,000 unstructured triangular elements in the water domain. The numbers of elements varied slightly when updating the geometry and the mesh to account for thermal swelling and mass loss of components due to evaporation. The mesh was refined near the outer surface of the droplet in order to capture the gradients of component mass fractions which are expected to be large at the short times in this region. The solution was performed using MATLAB code which calls COMSOL to solve the partial differential equation (PDE) in the problem described above. An iterative procedure was implemented to ensure the required precision of the results at each timestep. The aim of the procedure is to consider the variation in the physical properties during the timestep.

- **Step 0:** Physical properties of the liquid fuel, water and the gas phase are evaluated considering the state of the droplet at the end of the previous timestep.
- **Step 1:** The mass of each component m_i and the average temperature T_d are estimated at time $t_0 + dt$ using Eqs. (27) and (28).
- **Step 2:** The PDE problems for the heat transfer and component diffusion are solved using COMSOL considering the droplet geometry at time t_0. Functions T^a, T^b, Y_{li}^a and Y_{li}^b are calculated by resolving the problems described above.
- **Step 3:** Parameters α_T and α_i are evaluated from the values of m_i and T_d obtained in Step 1. The fields of temperature and component mass fractions are calculated using Eqs. (29) and (30).
- **Step 4:** The state of the droplet is determined at time $t_0 + dt$ using the fields of temperature and component mass fractions obtained in Step 3. The surface temperature (T_s), the average fuel temperature (T_f), the average water temperature (T_w), the surface component mass fractions (Y_{lis}), and average component mass fractions (Y_{lim}) are calculated. Then, the average state of the droplet between t_0 and $t_0 + dt$ is estimated as :

$$\bar{Z} = \frac{Z(t_0) + Z(t_0+dt)}{2}, \tag{41}$$

where $Z = T_s$, T_f, T_w, Y_{lis} or Y_{lim}. Raoult's law is used to determine the mass fraction of the vapour components Y_{vis} between the times t_0 and $t_0 + dt$.

- **Step 5:** The physical properties of the liquid fuel, water and the gas phase are evaluated for the average state defined in Step 4. Also, averaged values of R_w and R_d for each timestep are calculated using Eqs. (17) and (18).

Calculations return to Step 1 after Step 5 for a new iteration. To limit the computation time in the next iterations, PDE problems are not solved in COMSOL in Step 2. This has no effect on the results since it is assumed that thermal and mass diffusivities are constant and the geometry is fixed between times t_0 and $t_0 + dt$. Iterations are stopped when convergence is reached for the surface temperature $T_s(t_0+dt)$ and the mass fraction at the droplet surface ($Y_{lis}(t_0+dt)$). It is stipulated that $T_s(t_0 + dt)$ must not change by more than 0.1 K and Y_{lis} by more than 0.001 between the iterations. Finally, the geometry is updated to take into account the values of R_d and R_w obtained at time $t_0 + dt$. A new mesh is generated by calling COMSOL's meshing tools and the solutions obtained for the temperature and component mass fractions fields are projected onto this new mesh.

References

[1] Ogunkoya D, Li S, Rojas OJ, Fang T. Performance, combustion, and emissions in a diesel engine operated with fuel-in-water emulsions based on lignin. Appl Energy 2015;154:851–61. http://dx.doi.org/10.1016/j.apenergy.2015.05.036.

[2] Antonov DV, Kuznetsov GV, Strizhak PA. The micro-explosive fragmentation criteria of two-liquid droplets. Int J Heat Mass Transfer 2022;196:123293. http://dx.doi.org/10.1016/j.ijheatmasstransfer.2022.123293.

[3] Shinjo J, Xia J, Megaritis A, Ganippa LC, Cracknell RF. Modeling temperature distribution inside an emulsion fuel droplet under convective heating: a key to predicting microexplosion and puffing. At Sprays 2016;26:551–83. http://dx.doi.org/10.1615/AtomizSpr.2015013302.

[4] Shinjo J, Xia J, Ganippa LC, Megaritis A. Physics of puffing and microexplosion of emulsion fuel droplets. Phys Fluids 2014;26:103302. http://dx.doi.org/10.1063/1.4897918.

[5] Fostiropoulos S, Strotos G, Nikolopoulos N, Gavaises M. Numerical investigation of heavy fuel oil droplet breakup enhancement with water emulsions. Fuel 2020;278:118381. http://dx.doi.org/10.1016/j.fuel.2020.118381.

[6] Antonov DV, Strizhak PA, Fedorenko RM, Nissar Z, Sazhin SS. Puffing and micro-explosions in rapeseed oil/water droplets: the effects of coal micro-particles in water. Fuel 2021;289:119814. http://dx.doi.org/10.1016/j.fuel.2020.119814.

[7] Sazhin SS, Bar-Kohany T, Nissar Z, Antonov D, Strizhak PA, Rybdylova OD. A new approach to modelling micro-explosions in composite droplets. Int J Heat Mass Transfer 2020;161:120238. http://dx.doi.org/10.1016/j.ijheatmasstransfer.2020.120238.

[8] Castanet G, Antonov DV, Strizhak PA, Sazhin SS. Effects of water sub-droplet location on the start of puffing/micro-explosion in composite fuel-water droplets. Int J Heat Mass Transfer 2022;186:122466. http://dx.doi.org/10.1016/j.ijheatmasstransfer.2021.122466.

[9] Sazhin SS, Shchepakina E, Sobolev VA, Antonov DV, Strizhak PA. Puffing/micro-explosion in composite multi-component droplets. Int J Heat Mass Transfer 2022;184:122210. http://dx.doi.org/10.1016/j.ijheatmasstransfer.2021.122210.

[10] Abramzon B, Sirignano WA. Droplet vaporization model for spray combustion calculations. Int J Heat Mass Transfer 1989;32:1605–18. http://dx.doi.org/10.1016/0017-9310(89)90043-4.

[11] Antonov DV, Fedorenko RM, Strizhak PA, Castanet G, Sazhin SS. Puffing/micro-explosion of two closely spaced composite droplets in tandem: experimental results and modelling. Int J Heat Mass Transfer 2021;176:121449. http://dx.doi.org/10.1016/j.ijheatmasstransfer.2021.121449.

[12] Antonov DV, Volkov RS, Fedorenko RM, Strizhak PA, Castanet G, Sazhin SS. Temperature measurements in a string of three closely spaced droplets before the start of puffing/micro-explosion: Experimental results and modelling. Int J Heat Mass Transfer 2021;181:121837. http://dx.doi.org/10.1016/j.ijheatmasstransfer.2021.121837.

[13] Antonov DV, Fedorenko RM, Strizhak PA. Child droplets produced by micro-explosion and puffing of two-component droplets. Appl Therm Eng 2020;164:114501. http://dx.doi.org/10.1016/j.applthermaleng.2019.114501.

[14] Volkov RS, Kuznetsov GV, Strizhak PA. Temperature and velocity fields of the gas-vapor flow near evaporating water droplets. Int J Therm Sci 2018;134:337–54. http://dx.doi.org/10.1016/j.ijthermalsci.2018.08.029.

[15] Voytkov IS, Volkov RS, Lutoshkina OS, Kuznetsov GV. Temperature traces of water aerosols, water-based emulsions, solutions and slurries moving in a reversed flow of high-temperature gases. Exp Therm Fluid Sci 2018;98:20–9. http://dx.doi.org/10.1016/j.expthermflusci.2018.05.021.

[16] Sazhin SS. Droplets and sprays: Simple models of complex processes. London: Springer; 2022, http://dx.doi.org/10.1007/978-3-030-99746-5.